Comparative Medicine
Copyright 2014
by the American Association for Laboratory Animal Science

Vol 64, No 1
February 2014
Pages 25–33

Original Research

Comparison of 3 Real-Time, Quantitative Murine Models of Staphylococcal Biofilm Infection by Using In Vivo Bioluminescent Imaging

Kelly D Walton,[1] Allison Lord,[1] Lon V Kendall,[1,*] and Steven W Dow[1-3]

Biofilm formation represents a unique mechanism by which *Staphylococcus aureus* and other microorganisms avoid antimicrobial clearance and establish chronic infections. Treatment of these infections can be challenging, because the bacteria in the biofilm state are often resistant to therapies that are effective against planktonic bacteria of the same species. Effective animal models for the study of biofilm infections and novel therapeutics are needed. In addition, there is substantial interest in the use of noninvasive, in vivo data collection techniques to decrease the animal numbers required for the execution of infectious disease studies. To address these needs, we evaluated 3 murine models of implant-associated biofilm infection by using in vivo bioluminescent imaging techniques. The goal of these studies was to identify the model that was most amenable to development of sustained infections that could be imaged repeatedly in vivo by using bioluminescent technology. We found that the subcutaneous mesh and tibial intramedullary pin models both maintained consistent levels of bioluminescence for as long as 35 d after infection, with no implant loss experienced in either model. In contrast, a subcutaneous catheter model demonstrated significant incidence of incisional abscessation and implant loss by day 20 after infection. The correlation of bioluminescent measurements and bacterial enumeration was strongest with the subcutaneous mesh model. Among the 3 models we evaluated, the subcutaneous mesh model is the most appropriate animal model for prolonged study of biofilm infections by using bioluminescent imaging.

Abbreviation: BLI, bioluminescent imaging.

Staphylococcus aureus is a leading cause of cutaneous, pulmonary, bloodstream, and surgical infections worldwide. The growing prevalence of antimicrobial-resistant species in both hospital and community settings has inhibited therapeutic success considerably, resulting in increased rates of chronic and recurrent infections and rising healthcare costs.[1,3] More than half of all *S. aureus* isolates from hospital-acquired infections currently are classified as methicillin-resistant *S. aureus*, which are resistant to all β-lactam antimicrobials.[9] In addition, some strains of methicillin-resistant *S. aureus* have developed resistance to additional antimicrobial agents, including those previously reserved for multiply resistant organisms.[8]

One of the most complex resistance mechanisms of the *S. aureus* organism is the ability to form biofilms. The term biofilm refers to communities of bacterial cells that are organized within an extracellular polysaccharide matrix, which attaches to surfaces including indwelling medical devices and contaminated skin wounds. Organisms within a biofilm have increased protection from many components of the host's immune defenses as well as from exogenously administered antimicrobials, making this growth pattern a hallmark of chronic infection.[6] Due to variations among virulence factors expressed by biofilm organisms in comparison with their planktonic counterparts, therapies that are developed by using well-established models of septicemia or pneumonia may not be effective against biofilm infections involving the same species of bacteria.[1] The structure of the biofilm matrix itself further inhibits penetration and bacterial clearance by therapeutic compounds.[6] It is therefore of considerable interest to the biomedical research community to develop and evaluate reliable models of biofilm infections to facilitate the study of therapeutic candidates targeting this important defense mechanism.

Historically, the study of infectious disease has required euthanasia of large cohorts of animals at several experimental time points to enable tissue collection and culture. However, recent advances in in vivo imaging technology have established improved systems for studying these disease processes through noninvasive methods. Bioluminescent imaging (BLI) is often used to study tumor progression and metastasis, inflammation, and infection by using cells and organisms engineered to express the enzyme luciferase. This enzyme catalyzes a light-producing reaction that allows detection and image generation by specialized CCD cameras.[2,4] The bioluminescent signal emitted by metabolically active luciferase-expressing cells are detected by the CCD camera through the tissues of living animals, eliminating the need to euthanize subjects for bacterial quantification.[4] This advance not

Received: 05 Feb 2013. Revision requested: 16 Apr 2013. Accepted: 01 Aug 2013.
[1]Department of Microbiology, Immunology and Pathology, [2]Department of Clinical Sciences, and [3]Center for Immune and Regenerative Medicine, Colorado State University, Fort Collins, Colorado.
[*]Corresponding author. Email: lon.kendall@colostate.edu

only decreases the number of animals required to obtain statistically significant results but also reduces interindividual variability by allowing each animal to serve as its own control over time.

An effective model of biofilm infections that uses in vivo imaging technology must have several characteristics to permit accurate assessment of therapeutic efficacy in the setting of antimicrobial drug development. The model must be able to establish a reliable and robust infection capable of producing a strong bioluminescent signal of sufficient duration to allow the detection of differences between treated and untreated animals. In addition, complications such as the development of septicemia and implant loss should be minimal, because these events can significantly reduce sample size and result in the need to use additional animals. Furthermore, a useful model of biofilm infections must permit reliable correlation between bioluminescent signal measurement and actual bacterial counts.

The present study evaluated 3 previously described implant-associated infection models into which specific modifications have been incorporated to facilitate the use of BLI. These 3 models are the tibial intramedullary pin model, subcutaneous catheter model, and the subcutaneous mesh model. Each model has particular benefits for modeling certain aspects of chronic bacterial infection. We hypothesized that one of these models would prove most effective for adaptation to the BLI system of repeated evaluation of bacterial burden at the infection site over time.

Materials and Methods

Mice. Female ICR mice ($n = 30$; age, 6 to 8 wk) were purchased from a commercial supplier (Harlan Laboratories, Indianapolis, IN). Mice were housed in individually ventilated cages (Thoren Caging Systems, Hazleton, PA) at a density of 5 mice per cage and provided with free-choice irradiated rodent chow and sterile-filtered drinking water. Mice were serologically determined to be free of viral pathogens including mouse hepatitis virus, minute virus of mice, mouse parvovirus, enzootic diarrhea of infant mice virus, and Theiler murine encephalomyelitis virus. All animal procedures were reviewed and approved by the IACUC at Colorado State University.

Bacterial strain and implant preparation. Xen 36 (Caliper Life Sciences, Hopkinton, MA) is a bioluminescent strain of *S. aureus* genetically engineered to express a stable copy of a modified *Photorhabdus luminescens luxABCDE* operon, which encodes the enzyme luciferase (Caliper Life Sciences). Frozen bacterial stocks were stored at −80 °C and thawed in a 37 °C water bath prior to use; 500 µL of thawed Xen 36 *S. aureus* stock was cultured in 100 mL LB medium at 37 °C with agitation at 150 rotations per minute for 8 h to achieve log-phase growth prior to implant preparation.

Induction of infection. *Tibial intramedullary pin model.* Sections (length, 4 mm) of 0.25-mm sterilized stainless-steel insect pins were incubated in a Xen 36 *S. aureus* log-phase culture for 12 h at 37 °C and 150 rotations per minute. Pins were removed from the culture and rinsed thoroughly in sterile PBS prior to implantation.

Implant-associated osteomyelitis was initiated in 10 mice according to techniques previously described as a modification of the Norden model.[10,12,14,15] Briefly, mice were anesthetized with isoflurane, and the right hindlimb of each mouse was clipped of hair and aseptically cleansed with chlorhexidine and sterile water. A small incision was made over the medial aspect of the stifle joint to expose the proximal tibia, and pins coated with Xen 36 *S. aureus* were implanted transcortically into the intramedullary cavity. Mice received buprenorphine (0.05 mg/kg SC) immediately prior to the procedure and twice daily for the following 3 d.

Subcutaneous mesh implant model. Sections (each 6 mm × 6 mm) of sterile polypropylene surgical mesh (Surgipro, Tyco Healthcare, Princeton, NJ) were incubated in an overnight culture of Xen 36 *S. aureus* for 12 h at 37 °C and 150 rotations per minute. Mesh sections were removed from the culture and rinsed thoroughly with sterile PBS prior to implantation. Five identically treated mesh pieces were cultured on LB media immediately after preparation to determine the approximate bacterial inoculum.

Localized implant-associated infection was induced in 10 mice by using techniques adapted from a previously described murine biofilm model.[4] Briefly, mice were anesthetized with isoflurane, and a 2 × 2-cm area of the dorsum of each mouse was clipped of hair and aseptically cleansed with chlorhexidine and sterile water. A single dose of buprenorphine (0.05 mg/kg SC) was administered immediately prior to the procedure. A small dorsal midline incision was made on each mouse, and a subcutaneous pocket was created by using blunt dissection to the right lateral aspect of the incision. Sections of polypropylene mesh that were coated with Xen 36 *S. aureus* were implanted into the subcutaneous pockets, and the incisions were closed by using 2 stainless steel sterile wound clips.

Subcutaneous catheter model. Xen 36 *S. aureus* was incubated at 37 °C for 8 h to achieve log-phase growth and then diluted in LB broth to produce a solution containing 1×10^8 cfu per 50 µL. Localized catheter-associated infection was induced in 10 mice by using techniques adapted from a previously described murine biofilm model.[16,17] Briefly, mice were anesthetized with isoflurane, and a 2 × 2-cm area of the dorsum of each mouse was clipped of hair and aseptically cleansed with chlorhexidine and sterile water. A single dose of buprenorphine (0.05 mg/kg SC) was administered immediately prior to the procedure. A small, dorsal, midline incision was made on each mouse, and a subcutaneous pocket was created by using blunt dissection to the right lateral aspect of the incision. Sections (length, 5 mm) of sterile 14-gauge intravenous catheters (Abbocath-T, Hospira, Sligo, Ireland) were placed into the subcutaneous pockets, and the incisions were closed by using 2 stainless steel sterile wound clips. Xen 36 *S. aureus* (dose, 1×10^8 cfu) was injected percutaneously into the catheters prior to recovery from anesthesia.

In vivo BLI. Bioluminescence emitted from the infection site was quantified by using an in vivo imaging system (IVIS 100, Caliper Life Sciences). During the imaging procedure, mice were anesthetized with isoflurane to reduce movement, and procedures were standardized by using consistent exposure time, binning, and f/stop settings. Imaging occurred at regular intervals throughout the experiment until specified study endpoints were achieved. Specialized software (Living Image, Caliper Life Sciences) calculated light emission (no. of photons per second) within a designated region of interest.

Ex vivo bacterial quantification. *Tibial intramedullary pin model.* Mice were euthanized immediately prior to the final imaging session, and the operated tibias were harvested. Implants were removed, and the bones were homogenized in 2 mL sterile PBS. The pins then were placed into the bone homogenate, and bacteria were suspended in solution by using three 15-s intervals of

ice-cooled sonication. Serial dilutions were cultured on LB media for 24 h, and colonies counted to calculate total bacterial burden.

Subcutaneous mesh model. Mice were euthanized immediately prior to the final imaging session, and implants and the surrounding subcutaneous tissues were harvested. The tissue and implants from each animal were placed in individual 1-mL aliquots of sterile PBS and suspended in solution by using three 15-s intervals of ice-cooled sonication. Serial dilutions were cultured on LB media for 24 h and colonies counted to calculate total bacterial burden.

Subcutaneous catheter model. Mice were euthanized immediately prior to the final imaging session. Because all implants had been lost by 20 d after infection, bacterial counts could be determined only for mice euthanized on 8 d after infection. Implants and surrounding subcutaneous tissues from each animal were placed in individual 1-mL aliquots of sterile PBS and suspended in solution by using three 15-s intervals of ice-cooled sonication. Serial dilutions were cultured on LB media for 24 h, and colonies were counted to calculate total bacterial burden.

Histopathology. A single mouse per experimental group was euthanized each on days 8 and 35; tissues were harvested and fixed in 10% neutral buffered formalin (VWR, West Chester, PA**)**. For mice infected by using either the subcutaneous catheter or subcutaneous mesh implants, skin samples including the implant and surrounding abscess were harvested. Tibias were collected from mice infected by using intramedullary pins, cleaned of the surrounding soft tissue, and placed in decalcifying solution (Richard-Allan Scientific, Kalamazoo, MI) for 24 h prior to fixing. All implants were removed before further processing. Tissues were paraffin-embedded, and 5-µm sections were applied to glass slides and stained with hematoxylin and eosin for routine histopathologic analysis. To identify additional characteristic features of biofilm formation, Gram and periodic acid–Schiff stains were used.

Statistical analysis. Differences in bioluminescence over time between groups were analyzed for statistical significance by using 2-way ANOVA with Bonferroni multiple-comparisons post-tests. Correlation between photon flux and bacterial counts was calculated by using a Spearman correlation test. A Student *t* test was used to characterize the difference in final bacterial numbers between the intramedullary pin and subcutaneous mesh groups on day 35 after infection. All statistical analyses were performed by using a commercial scientific graphing and biostatistics software package (GraphPad Prism, La Jolla, CA). A *P* value of 0.05 or less was considered to indicate a statistically significant result for all analyses.

Results

BLI. Implant-associated *S. aureus* biofilm infections were induced in 10 mice for each of the 3 models studied (intramedullary pin, subcutaneous catheter, and subcutaneous mesh), and disease progression was monitored by using BLI every 2 to 3 d. At 8 d after infection, 5 mice per group were euthanized for bacterial quantification, and the remaining mice continued to be monitored until day 35 after infection. The average bioluminescent measurement of the intramedullary pin group on day 35 after infection was approximately 0.7 $\log_{10}$ lower ($P = 0.06$) than that of the subcutaneous mesh group. Decreases in bioluminescence from day 1 after infection to day 35 after infection in the subcutaneous mesh and intramedullary pin groups were 0.986 $\log_{10}$ and 0.755 $\log_{10}$, respectively (Figure 1 A). On day 35 after infection, the average bioluminescence in the intramedullary pin group was approximately 48% of the original measurement on day 1, whereas the average bioluminescence in the subcutaneous mesh group was approximately 8% of the original value (Figure 1 B). Bioluminescent measurements were calculated from light emission within a defined region of interest (Figure 2).

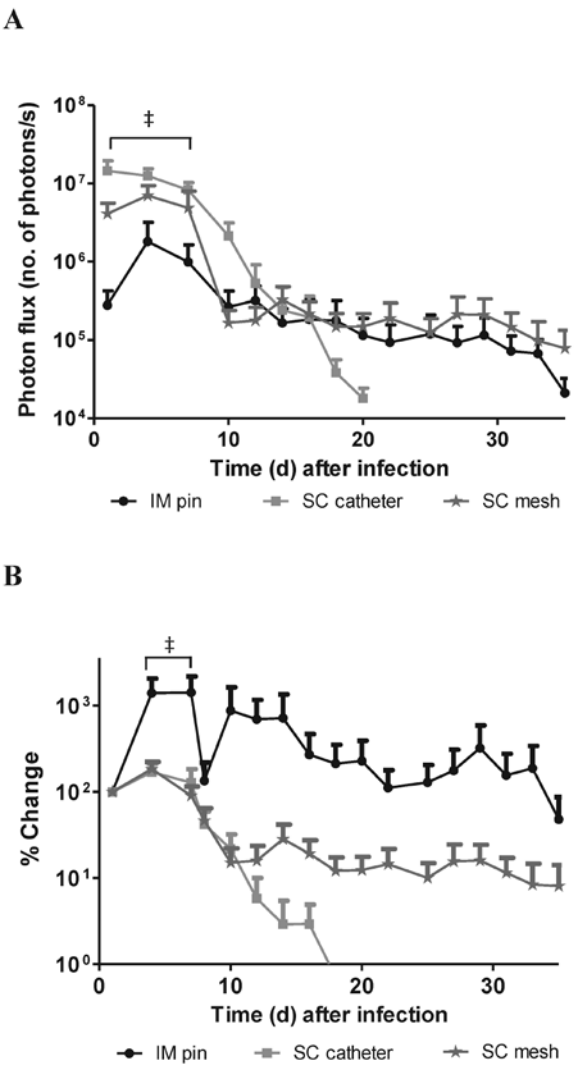

Figure 1. Time course of bioluminescence emission. (A) Bioluminescence measurements are presented as group means ± SEM over the 35-d study period. (B) Bioluminescence measurements are expressed as a percentage of the initial measurement on day 1 after infection (100% for all groups) to demonstrate relative changes in light emission over time. ‡, Signifcant ($P < 0.001$) difference between values for groups 1 and 3 compared with group 2 on days 1, 4, and 7 after infection.

Correlation between BLI and bacterial burden according to results of direct plating. Biofilms were removed from explanted materials and cultured on LB media for 24 h to determine the total bacterial burden associated with each implant. The mean number of colony-forming units (cfu) isolated from pins was 6.953×10^8 at day 8 and 1.910×10^6 at day 35. Catheters yielded a mean of 9.455×10^9 cfu at day 8 and meshes produced 2.385×10^9 cfu at day 8 and 1.711×10^4 cfu at day 35. On day 35, the difference in mean numbers of cfu was significant ($P < 0.05$) between the intramedullary pin group and the subcutaneous mesh group.

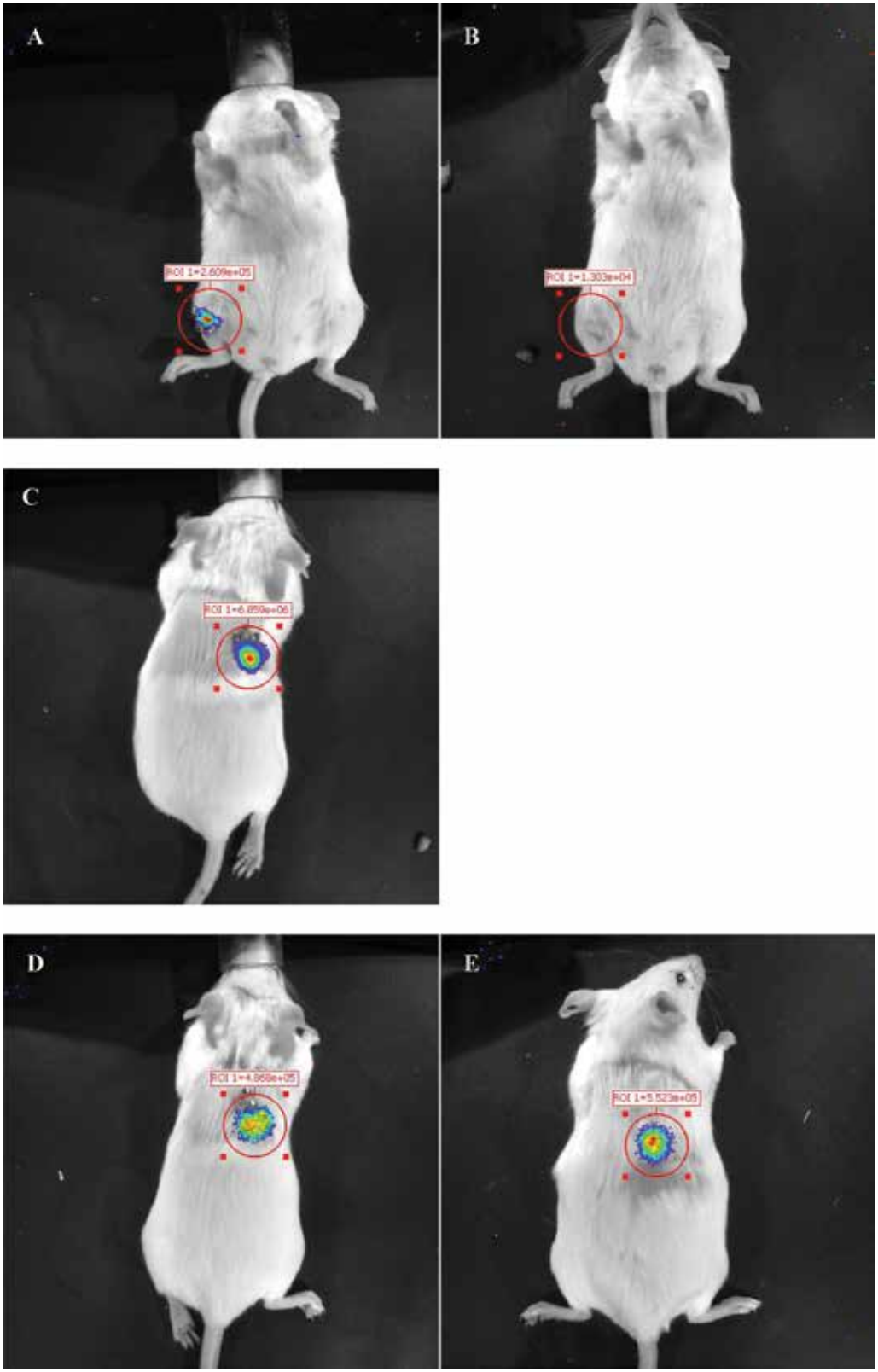

Figure 2. Bioluminescent images and light emission from designated region of interest. (A) Intramedullary pin on day 8 after infection. (B) Intramedullary pin on day 35 after infection. (C) Subcutaneous catheter on day 8 after infection. (D) Subcutaneous mesh on day 8 after infection. (E) Subcutaneous mesh on day 35 after infection.

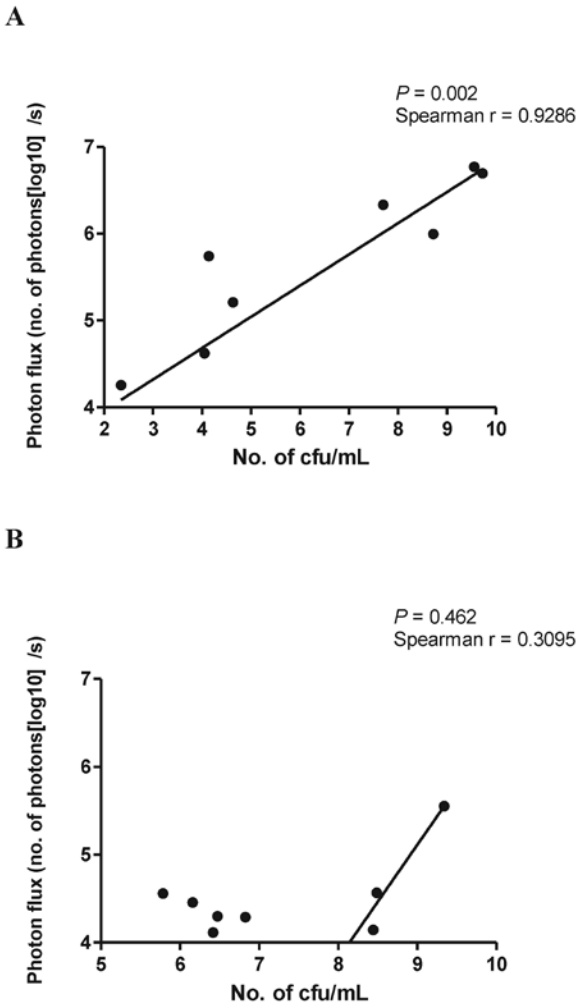

Figure 3. Correlation between BLI signal intensity and bacterial burden as determined by direct plating. After the final imaging session, biofilms were harvested from explanted (A) meshes and (B) pins for determination of colony counts. Colony counts were plotted against bioluminescence measurements (no. of photons/s) and analyzed for correlation.

The relationship between bacterial counts and end-point bioluminescent measurements was characterized by using a Spearman correlation test, which demonstrated that a strong correlation existed between bacterial numbers and photon measurements for the subcutaneous mesh model ($P = 0.002$, Spearman $r = 0.9286$; Figure 3 A) but not for the intramedullary pin model ($P = 0.462$, Spearman $r = 0.3095$; Figure 3 B). Statistical correlation did not exist for the subcutaneous catheter model at 8 d after infection ($P = 0.3333$, Spearman $r = 0.8$); because all implants had been lost by day 35 after infection, correlation was not calculated for this time point.

Histopathologic analysis. ***Tibial intramedullary pin model.*** Microscopically, osteomyelitis at day 8 after infection was characterized by an inflammatory infiltrate predominately composed of neutrophils and macrophages, marked fibroplasia, and an increase in granulocytic precursors within the marrow cavity (Figure 4 A and B). By day 35 after infection, the infiltrate was increasingly suppurative in nature, with the presence of degenerative neutrophils, fibrinous granules, and abundant necrotic cellular debris. A wispy basophilic matrix, suggestive of neutrophilic extracellular entrapment, was found interwoven among regions of fibroplasia and inflammation (Figure 4 C, arrow). The inflammatory infiltrate invaded the adjacent musculature, and the affected bone trabeculae demonstrated a roughened appearance with bacterial colonies apparent along the bone surface (Figure 4 C and D, arrow). An area of fibroplasia was evident at the periphery of the lesion.

Subcutaneous mesh model. At day 8 after infection, an area of ulceration was present at the dermal surface and had a serocellular crust consisting of neutrophils, keratin, serum, cellular debris, and bacterial colonies (Figure 5 A, black arrow). The adjacent epidermis was hyperplastic with orthokeratotic hyperkeratosis. There was a marked infiltrate of neutrophils, macrophages, and fibroblasts in the subcutaneous tissue which moderately expanded the subcutaneous adipocytes and underlying panniculus muscles (Figure 5 A, white arrow). On day 35 after infection, there was marked dermal fibrosis with minimal inflammation and aggregates of lymphocytes in the subcutaneous tissue (Figure 5 B).

Subcutaneous catheter model. On day 8 after infection, severe ulceration with a similar cell population as described for the mesh implant was present, with an increased inflammatory cell component (Figure 6 A). In addition, numerous bacterial colonies with frequent sulfur granule formation (Figure 6 B, white arrow) and wispy basophilic matrix suggestive of neutrophilic extracellular entrapment (Figure 6 B, black arrow) were noted within the subcutaneous tissues. The underlying dermis was markedly expanded by an infiltrate of neutrophils, macrophages, and fibroblasts which extended into the panniculus muscles (Figure 6 C). All implants had been lost by day 20 after infection.

Gram and periodic acid–Schiff stains of tissues from all 3 models demonstrated tightly adhered gram-positive bacterial colonies in close association with tissue surfaces. In some cases, these colonies were weakly positive by periodic acid–Schiff staining, indicating the presence of polysaccharide within the matrix. These findings support the formation of biofilms on contaminated implants harvested from mice.

Implant loss. During the postinfection period, mice were monitored every 2 d for bioluminescence, incisional abscessation or dehiscence, and the ability to palpate subcutaneous implants. Implant loss was declared when a sudden, dramatic decrease in bioluminescence was detected, in conjunction with the presence of incisional abscessation or dehiscence and the inability to palpate a subcutaneous implant. Implant loss was confirmed at experimental endpoints after ex vivo collection (days 8 and 35 after infection). Mice in the intramedullary pin and subcutaneous mesh groups experienced no incidence of implant loss over the course of the experiment. Compared with other groups, subcutaneous catheter mice experienced 100% implant loss by day 20 after infection, with some catheter loss occurring as early as day 8 ($P < 0.05$).

Discussion

Reliable animal models of infectious diseases are challenging to develop and implement and frequently require large numbers of animals to collect sufficient data at critical time points after infection. The use of in vivo BLI can significantly reduce animal

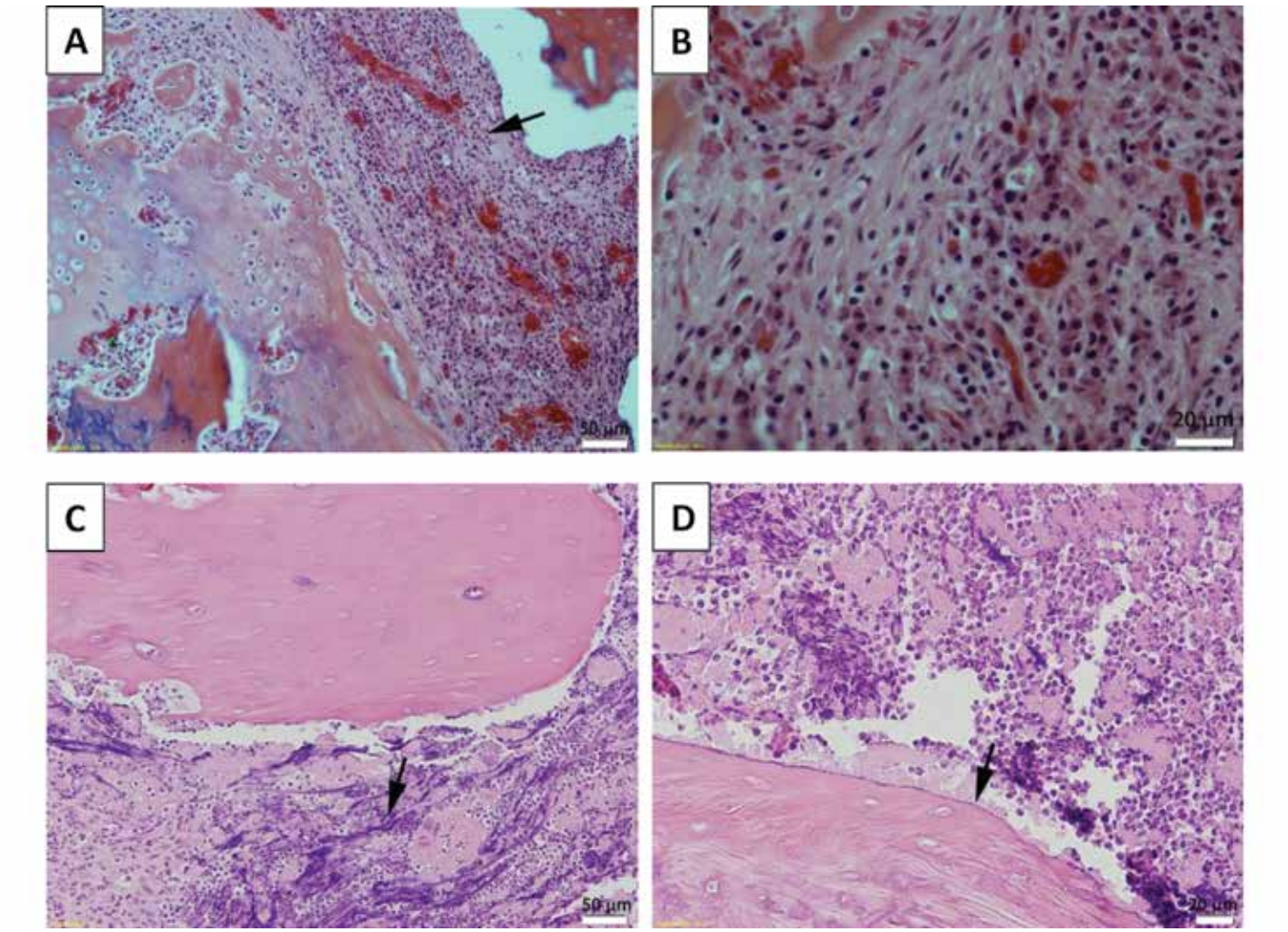

Figure 4. Photomicrographs of tibia bones from mice implanted with *S. aureus*-coated intramedullary pins. (A and B) Osteomyelitis characterized by an infiltration of neutrophils and macrophages with fibroplasia (arrow). (C) Day 35 after infection. The inflammatory infiltrate is predominately composed of degenerative neutrophils. A basophilic matrix suggestive of neutrophilic extracellular entrapment is present within areas of inflammation (arrow). (D) Bacterial colonies are apparent along the bone surface (arrow). Hematoxylin and eosin stain.

numbers and associated expenses by allowing noninvasive, real-time in vivo data collection over the course of the study period. Limitations of this technology exist when the actual bacterial burden is insufficient to elicit a robust bioluminescent signal or when the host immune system is able to clear the infection readily without the assistance of standard or experimental therapeutics. Of utmost importance is the ability to effectively correlate the bioluminescent measurement with actual bacterial counts, which may vary among the different biofilm models.

The 3 models of *S. aureus* biofilm infections we evaluated here each have attributes that may be useful in a variety of studies examining bacterial infection pathogenesis, virulence, or novel therapeutics. Chronic infections, including those involving biofilm development, are characterized by long duration (weeks to months) and persistence of infectious organisms. The ability to accurately model the important features of chronic infection is critical for preclinical assessment of experimental drugs. An animal model that does not provide ideal conditions for disease development or that permits efficient bacterial clearance by the host immune system in untreated subjects is unlikely to deliver reliable results in these studies.

Our results show that the subcutaneous mesh and intramedullary pin models maintained stable infections that could be detectable via BLI for at least 35 d after infection, indicating that these models may be useful tools for long-term studies of chronic bacterial implant infections. The average bioluminescent measurement in the subcutaneous mesh group was slightly higher than that in the intramedullary pin group, suggesting that the subcutaneous mesh model may provide improved opportunity for the detection of differences among groups in treatment studies.

All mice in the subcutaneous catheter group experienced incisional abscessation or dehiscence with subsequent implant loss by day 20 after infection. This observation indicates that the subcutaneous catheter model, as described here, is unlikely to be useful in studies of longer duration. Incisional abscessation and implant loss was a complication unique to the subcutaneous catheter group. This finding may suggest that the animals in

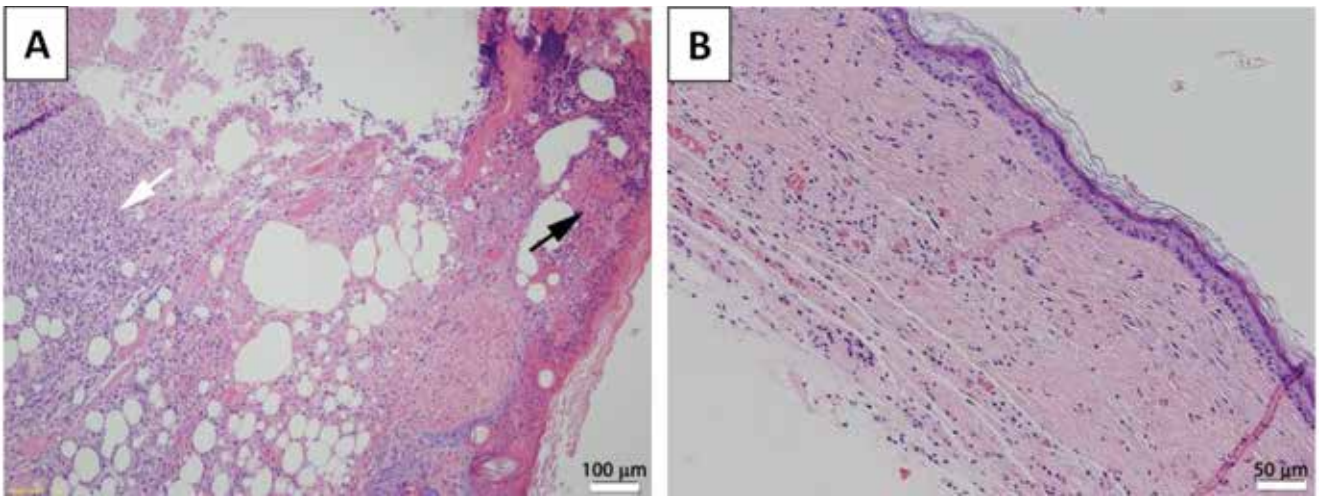

Figure 5. Photomicrographs of skin and subcutaneous tissues collected from the infection site of mice infected via the subcutaneous catheter route. (A) Day 8 after infection. An area of ulceration and serocellular crusting is present on the surface of the skin. The crust consists of neutrophils, keratin, serum, cellular debris and bacterial colonies (black arrow). A marked cellular infiltrate composed predominately of neutrophils, macrophages, and fibroblasts is observed within the subcutaneous tissue (white arrow). (B) Day 35 after infection. Marked dermal fibrosis with minimal inflammation and aggregates of lymphocytes can be seen within the subcutaneous tissue. Hematoxylin and eosin stain.

this group received a greater initial bacterial inoculum than did the other 2 groups; however, culturing of biofilms removed from nonimplanted meshes determined that the inoculum was similar among both subcutaneous implant groups. A more likely explanation may involve the percutaneous delivery of bacteria into the implant in this model. Because the inoculum for the catheter model was fluid and not immediately adhered to the implant as in the subcutaneous mesh and intramedullary pin models, there may have been an increased risk for incisional contamination due to bacterial dispersion.

At necropsy, mesh implants were found to be surrounded by a thick, fibrous capsule, a finding that was not consistent in the subcutaneous catheter model. This result was presumably related to dispersion of the inoculum in the mice with subcutaneous catheter implants, inhibiting the development of a host reaction to effectively 'wall off' the infection and allowing the bacteria to replicate more readily. This effect may be a potential explanation for the increased inflammation, dermal ulceration, and bacterial growth observed histologically in the subcutaneous catheter group. The success of this model might have been improved if a lower concentration of initial inoculum had been used or if the catheter was precoated with *S. aureus* prior to implantation, as done in other models described.[7]

The correlation of bioluminescent measurements with actual bacterial counts is a key consideration for the use of BLI. Numerous previous studies[4,5,7] illustrate a strong correlation between these 2 measurements, but diverse factors can interfere with the ability of an imaging system to provide an accurate estimation of bacterial burden. For example, morphologic characteristics of the animal, such as skin pigmentation and fur, can interfere with the emission of light from the infection site and result in decreased bioluminescent signals. To reduce the effect of these factors, we used albino mice in the current experiments, and we clipped the fur as needed prior to imaging.

We obtained lower bioluminescent measurements in mice with intramedullary pin implants compared with mice with subcutaneous mesh implants at 35 d after infection; however, ex vivo culture demonstrated that mice in the intramedullary pin group actually had significantly ($P = 0.0131$) higher bacterial numbers than did mice in the subcutaneous mesh group. Histopathologic analysis supported this finding, with evidence of marked bacterial osteomyelitis that subjectively did not appear to correspond with relatively low bioluminescence measurements in the intramedullary pin group. Statistical analysis revealed that total bacterial numbers recovered from subcutaneous mesh implants correlated strongly with the respective imaging data ($P = 0.002$, Spearman $r = 0.9286$), whereas the correlation between bacterial counts and photons from the intramedullary pins was not significant ($P = 0.462$, Spearman $r = 0.3095$). These findings suggest that some characteristic of the intramedullary pin model may have inhibited the emission of light, resulting in artifactually decreased bacterial estimation. One possibility for this discrepancy is that the stainless steel pin implant may have absorbed more light than did the other 2 types of implants, effectively reducing the radiance that can be detected by the CCD camera. Specific properties of bone, such as mineral components, may similarly inhibit light production, but we know of no prior scientific data to support this theory.[5,13] This lack of convincing correlation between bioluminescence and bacterial counts indicates that the intramedullary pin model would be more useful in conventional studies than in those that involve BLI.

It is important to note that there are some specific differences between the intramedullary pin infection model and the subcutaneous mesh model that should be considered during the model selection process. Osteomyelitis is an especially challenging infection to treat, because of the anatomic location and physical characteristics of bone that result in reduced penetration by antimicrobial drugs. Therefore, osteomyelitis pathogenesis and treatment can be considered an area of research that is independent from all others, and subcutaneous implant models would be of little value in these investigations. In these cases, the intramedullary pin model is a valuable tool that should be considered, given that our current study and others have demonstrated that it effectively mimics characteristics of these infections in a clinical setting.[5,10,12,14,15] In

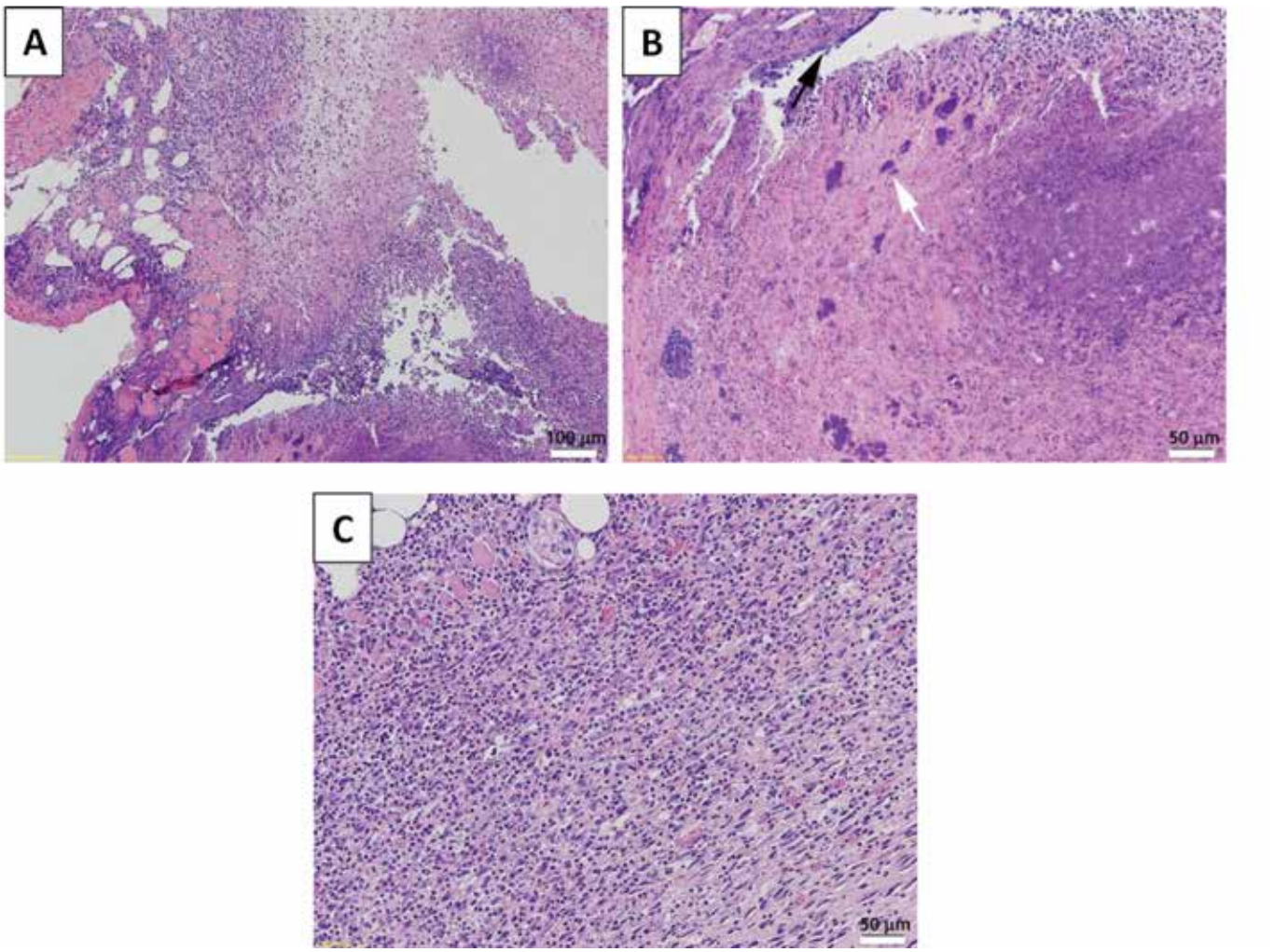

Figure 6. Photomicrographs of skin and subcutaneous tissues collected from the infection site of mice implanted with *S. aureus*-coated mesh. (A) Day 8 after infection. There is severe dermal ulceration and subcutaneous cellular infiltration of neutrophils, macrophages, and fibroblasts. (B) Increased bacterial colonies are frequently seen with sulfur granule formation (white arrow) and basophilic matrix suggestive of neutrophilic extracellular entrapment (black arrow). (C) The underlying dermis is markedly expanded by an infiltrate of neutrophils, macrophages and fibroblast which extends into the panniculus muscles. Hematoxylin and eosin stain.

addition, other groups have successfully conducted studies using these models of osteomyelitis in conjunction with BLI.[5,11] The main complication experienced with the intramedullary pin model in the present study was related not to the fact that the bones appeared to emit lower levels of bioluminescence than did the subcutaneous implant models, given that this apparent discrepancy can partially be explained by differences in tissue density or depth.[2] Rather, our concern was that we were unable to reliably correlate bacterial numbers recovered from explanted bones with bioluminescence measurements obtained prior to harvest.

We determined that the subcutaneous mesh model that we describe here is an effective and reliable tool for studying staphylococcal biofilm infections in conjunction with BLI. We found that this model was significantly better than was the subcutaneous catheter model in terms of implant retention and sustained imaging. Furthermore, although the intramedullary pin model reliably produced stable infections over the course of the experimental period, the subcutaneous mesh model demonstrated superior correlation between bioluminescence and bacterial counts. Future studies should explore the use of the subcutaneous mesh model for the evaluation of novel therapeutics and treatment protocols for biofilm infections.

Acknowledgments

This work was supported in part by the College of Veterinary Medicine and Biomedical Sciences (CVMBS) College Research Council Animal Health and Disease Funds and the Infectious Disease SuperCluster. We thank Laura Chubb for her assistance with the operation of the IVIS 100 imaging system.

References

1. **Brady RA, O'May GA, Leid JG, Prior ML, Costerton JW, Schirtliff ME.** 2011. Resolution of *Staphylococcus aureus* biofilm infection using vaccination and antibiotic treatment. Infect Immun **79:**1797–1803.
2. **Contag CH, Ross BD.** 2002. It's not just about anatomy: in vivo bioluminescence imaging as an eyepiece into biology. J Magn Reson Imaging **16:**378–387.

3. **Cosgrove SE.** 2006. The relationship between antimicrobial resistance and patient outcomes: mortality, length of hospital stay, and healthcare costs. Clin Infect Dis **42:**S82–S89.
4. **Engelsman AF, van der Mei HC, Francis KP, Busscher HJ, Ploeg RJ, van Dam GM.** 2009. Real time noninvasive monitoring of contaminating bacteria in a soft-tissue implant infection model. J Biomed Mater Res B Appl Biomater **88:**123–129.
5. **Funao H, Ishii K, Nagai S, Sasaki A, Hoshikawa T, Aizawa M, Okada Y, Chiba K, Koyasu S, Toyama Y, Matsumoto M.** 2012. Establishment of a real-time, quantitative, and reproducible mouse model of staphylococcal osteomyelitis using bioluminescence imaging. Infect Immun **80:**733–741.
6. **Gotz F.** 2002. *Staphylococcus* and biofilms. Mol Microbiol **43:**1367–1378.
7. **Kadurugamuwa JL, Sin L, Albert E, Yu J, Francis K, DeBoer M, Rubin M, Bellinger-Kawahara C, Parr Jr TR Jr, Contag PR.** 2003. Direct continuous method for monitoring biofilm infection in a mouse model. Infect Immun **71:**882–890.
8. **Kim HK, Cheng AG, Kim HY, Missiakas DM, Scneewind O.** 2010. Nontoxigenic protein A vaccine for methicillin-resistant *Staphylococcus aureus* infections in mice. J Exp Med **207:**1863–1870.
9. **Klevens RM, Edwards JR, Gaynes RP, System NNIS; National Nosocomial Infections Surveillance System.** 2008. The impact of antimicrobial-resistant, healthcare-associated infections on mortality in the United States. Clin Infect Dis **47:**927–930.
10. **Li D, Gromov K, Soballe K, Puzas JE, O'Keefe RJ, Awad H, Drissi H, Schwarz EM.** 2008. A quantitative mouse model of implant-associated osteomyelitis and the kinetics of microbial growth, osteolysis, and humoral immunity. J Orthop Res **26:**96–105.
11. **Niska JA, Meganck JA, Pribaz JR, Shahbazian JH, Lim E, Zhang N, Rice BW, Akin A, Ramos RI, Bernthal NM, Francis KP, Miller LS.** 2012. Monitoring bacterial burden, inflammation, and bone damage longitudinally using optical and μCT imaging in an orthopaedic implant infection in mice. PLoS ONE **7:**e47397.
12. **Norden CW.** 1970. Experimental osteomyelitis. I: a description of the model. J Infect Dis **122:**410–418.
13. **Reumann MK, Weiser MC, Mayer-Kuckuk P.** 2010. Musculoskeletal molecular imaging: a comprehensive overview. Trends Biotechnol **28:**93–101.
14. **Shandley S, Matthews KP, Cox J, Romano D, Abplanalp A, Kalns J.** 2012. Hyperbaric oxygen therapy in a mouse model of implant-associated osteomyelitis. J Orthop Res **30:**203–208.
15. **Tsiolis P, Giamarellos-Bourboulis EJ, Mavrogenis AF, Savvidou O, Lallos SN, Frangia K, Lazarettos I, Nikolou V, Efstathopoulos NE.** 2011. Experimental ostemyelitis caused by methicillin-resistant *Staphylococcis aureus* treated with a polyactide carrier-releasing linezolid. Surg Infect (Larchmt) **12:**131–135.
16. **Vergara-Irigaray M, Valle J, Merino N, Latasa C, Gargia B, Ruiz de los Mozos I, Solano C, Toledo-Arana A, Penades JR, Lasa I.** 2009. Relevant role of fibronectin-binding proteins in *Staphylococcus aureus* biofilm-associated foreign body infections. Infect Immun **77:**3978–3991.
17. **Weiss EC, Zielinska A, Beenken KE, Spencer HJ, Daily SJ, Smeltzer MS.** 2009. Impact of *sarA* on daptomycin susceptibility of *Staphylococcus aureus* biofilms in vivo. Antimicrob Agents Chemother **53:**4096–4102.